Journal of Energy Chemistry 28 (2019) 123–127

Contents lists available at ScienceDirect

Journal of Energy Chemistry

journal homepage: www.elsevier.com/locate/jechem

http://www.journals.elsevier.com/journal-of-energy-chemistry/

Communication

Enhanced hydrogen evolution reaction over molybdenum carbide nanoparticles confined inside single-walled carbon nanotubes

Tingting Cui[a,b,1], Jinhu Dong[a,b,1], Xiulian Pan[a,*], Tie Yu[a], Qiang Fu[a], Xinhe Bao[a,*]

[a] State Key Laboratory of Catalysis, Dalian Institute of Chemical Physics, Chinese Academy of Sciences, Dalian 116023, Liaoning, China
[b] University of Chinese Academy of Sciences, Beijing 100049, China

ARTICLE INFO

Article history:
Received 9 February 2018
Revised 14 March 2018
Accepted 18 March 2018
Available online 22 March 2018

Keywords:
Single-walled carbon nanotubes
Confined catalysis
Molybdenum carbide
Nanoparticles
Hydrogen evolution reaction

ABSTRACT

Carbon nanotubes (CNTs) have shown as unique nanoreactors to tune the catalytic activity of confined nano-catalysts. Here we report that the catalytic performance of molybdenum carbide nanoparticles (MoC_x NPs) for the hydrogen evolution reaction (HER) process can be enhanced by encapsulation within single-walled carbon nanotubes (SWNTs) with a diameter of 1–2 nm. The catalyst with MoC_x NPs located on the interior surface of SWNTs (MoC_x@SWNTs) exhibits a lower onset over-potential and a smaller Tafel slope than the one with MoC_x NPs attached on the exterior surface (MoC_x/SWNTs). This is likely attributed to the much smaller particle size and the more reduced states of the confined MoC_x NPs, as well as the larger specific surface area of MoC_x@SWNTs compared with MoC_x/SWNTs. In addition, the electronic structure of the confined MoC_x NPs might be modified by the confinement effects of SWNTs, and hence the adsorption free energy of H atoms on the confined MoC_x NPs, which could also contribute to their higher performance. These results suggest that the SWNTs can be further explored for constructing novel catalysts with beneficial catalytic performance.

Hydrogen is considered as an ideal energy carrier alternative to the traditional fossil resources due to its renewable and clean nature [1,2]. Electrochemical water splitting is a promising method for H_2 generation due to its high efficiency [3]. Wide efforts have been devoted to developing active catalysts for the aqueous hydrogen evolution reaction (HER) process [4–8]. Pt-based catalysts remain the most efficient HER electro-catalysts so far. However, the high cost and low abundance of Pt limit its large-scale applications. Hence the development of other low-cost and highly efficient HER catalysts has driven continuous efforts in this field [9,10]. A series of earth-abundant 3*d*-trasition metal-based materials including carbides [11–13], disulfides [14], nitrides [15], and phosphides [16] have been reported as the good HER catalysts.

Among them, transition metal carbides, especially molybdenum carbide (MoC_x), have been investigated intensively in recent years for their abundance and Pt-like electronic structure [11,17]. However, bulky Mo-based carbide exhibited unsatisfactory performance in both acidic and basic conditions as reported earlier [18]. Thus, carbides with different nanostructures have been constructed in order to optimize the performance [19]. For example, small sized MoC_x nanoparticles (NPs) coated by few layers of carbon atoms showed an excellent HER activity over a wide pH range and long term stability, e.g., the over-potential (η) is as low as 124 mV at the current density of 10 mA cm^{-2} at pH = 0 [20]. Hierarchical β-Mo_2C nanotubes, fabricated through an unusual template-engaged strategy, exhibited a low onset potential of 82 mV at pH = 0 due to the large surface area, fast charge transfer and unique tubular structure of the catalyst [21]. MoC/Mo_2C hetero-nanowires obtained via controlled carbonization, presented a lower onset potential of 38 mV and 20 h long-term durability in acidic electrolytes [22]. However, it remains a challenge to obtain highly dispersed MoC_x NPs because a relatively harsh carbonization temperature (>700 °C) is usually required to carbonize Mo species. Moreover, small MoC_x NPs are usually very active and prone to oxidation when exposed to the air. Our previous studies showed that metal nanoparticles encapsulated within the nano-channels of carbon nanotubes (CNTs) were protected and less prone to oxidation, tending to retain a more reduced state due to confinement effects [23,24]. Furthermore, the relatively rigid space of the CNT channels could exert physical restriction, alleviating the aggregation of nanoparticles even under reaction conditions. We wonder if the confinement effects can be employed for synthesis of well dispersed MoC_x NPs and study its effects on HER. Therefore, we dispersed MoC_x NPs in the inner cavity

* Corresponding authors.
E-mail addresses: panxl@dicp.ac.cn (X. Pan), xhbao@dicp.ac.cn (X. Bao).
[1] These authors contributed equally to this work.

https://doi.org/10.1016/j.jechem.2018.03.006
2095-4956/

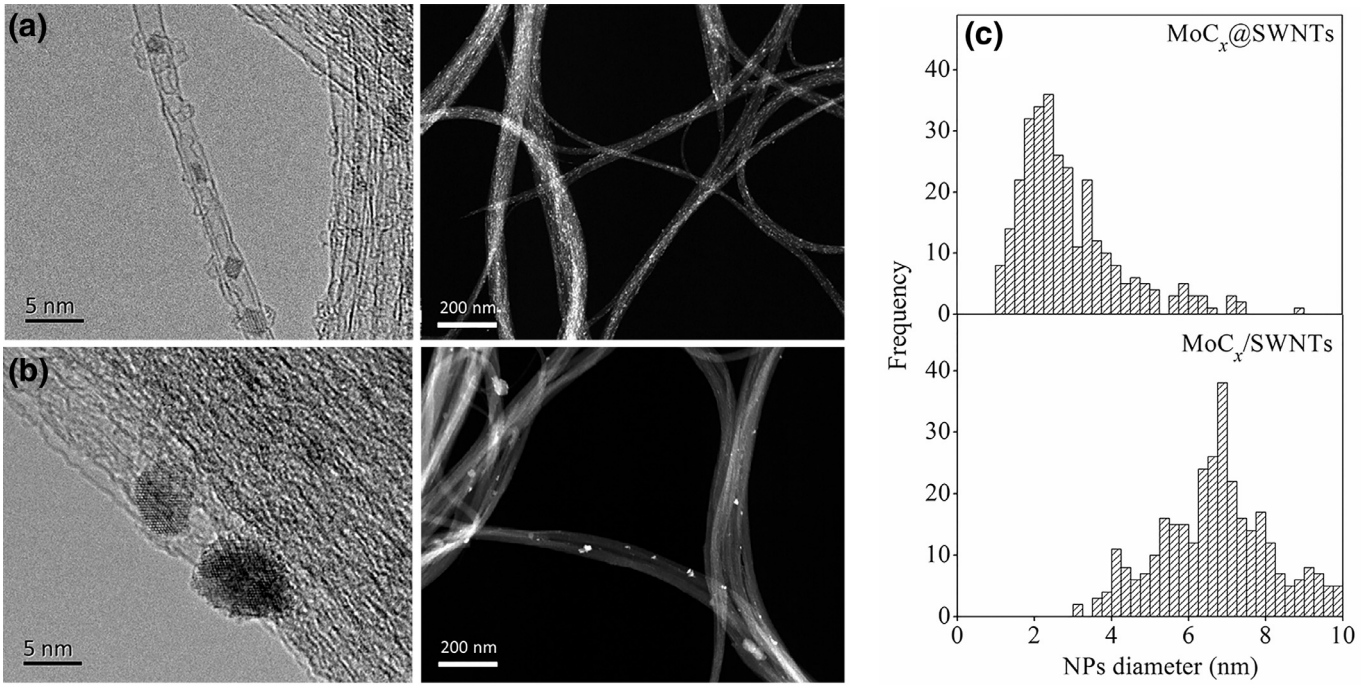

Fig. 1. HRTEM and HAADF-STEM images of (a) MoC$_x$@SWNTs and (b) MoC$_x$/SWNTs; (c) particle size distribution of MoC$_x$ measured from 200 NPs [25].

of single-walled carbon nanotubes (SWNTs) with a diameter of 1–2 nm. The results show that the HER activity of MoC$_x$ NPs can be enhanced by encapsulation within the channels of SWNTs with respect to those NPs dispersed on the exterior walls of SWNTs.

The preparation methods for the SWNTs encapsulated MoC$_x$ catalyst and those dispersed on the exterior walls of SWNTs have been reported previously [25]. Briefly, SWNTs were first evacuated to 10^{-4} Pa at 450 °C and then were exposed to cycloheptatriene molybdenum tricarbonyl ($C_7H_8Mo(CO)_3$) vapor. The mixture was kept under 100 °C for 24 h in a sealed reactor. Then Mo species were deposited inside the SWNT channels by forming oxide upon treatment in atmospheric air at 100 °C. Subsequently, the sample was treated with 0.25 M HNO_3 to remove the molybdenum species on the outer walls followed by washing in deionized water. The resulting composite was calcined in pure Ar at 800 °C for 2 h to obtain carbides (denoted as MoC$_x$@SWNTs). For comparison, MoC$_x$ NPs were also deposited on the outer walls of SWNTs (denoted as MoC$_x$/SWNTs), which were prepared by wetness incipient impregnation with toluene as the solvent. All the other conditions and chemicals were kept the same as for preparation of MoC$_x$@SWNTs including the precursors and the same batch SWNTs. The electrochemical properties were evaluated using a standard three-electrode cell (AKCELL3, Pine Research Instrumentation) at room temperature (25 °C) in 1 M $HClO_4$ aqueous solution. An Ag/AgCl electrode (Saturated KCl, Shanghai Leici Electronic Technology Co., Ltd) and a Pt-wire electrode (Wuhan Gaoss Union Co., Ltd.) were used as reference electrode and counter electrode, respectively. The rotation rate and the potential of working electrode were controlled by an MSR Electrode Rotator (Pine Research Instrumentation) and a CH Instrument potentiostat (CHI 660E). The potential correction between the Ag/AgCl reference electrode and reversible hydrogen electrode (RHE) was 0.201 V. Typically, 5 mg catalyst powder and 50 μL Nafion aqueous solution (5 wt%, Dupont) were dispersed in 2 mL ethanol to form a homogeneous ink under ultrasonication. 25 μL ink was carefully dropped on the commercial glassy carbon electrode (GCE, AFE5050GC, 5 mm in diameter, 0.196 cm^2, Pine Research Instrumentation) with a micropipette and dried in air at room temperature. Linear sweep voltammetry (LSV) was conducted in Ar-saturated 1 M $HClO_4$ solution with a scan rate of 2 mV s^{-1}. The hydrogen evolution reaction (HER) activity was recorded using rotating disc electrode (RDE) measurement at a rotation rate of 2500 rpm at 25 °C.

The particle size distribution of MoC$_x$@SWNTs has been reported in the previous study [25], which has been obtained by statistical study of 200 MoC$_x$ NPs from the randomly scanned high-resolution transmission electron microscopy (HRTEM, JEOL JEM-2100, 200 kV) and high angle annular dark field scanning transmission electron microscopy (HAADF-STEM, FEI Titan 80-300, 300 kV) specimen. The result showed that more than 80% of the NPs fall in a size range of 1.0–4.0 nm with an average of 2.9 nm [25]. By using the same statistical method based on HRTEM and HAADF-STEM examination, we obtained the particle size distribution of MoC$_x$/SWNTs (Fig. 1). The results show that MoC$_x$ NPs located on the exterior walls of SWNTs exhibit a much larger size of 4.0–9.0 nm with an average of 6.5 nm. This demonstrates the importance of the space confinement of the SWNT channels, which can restrict the aggregation of Mo species during the high temperature carburization process (800 °C). Furthermore, our previous study using HRTEM and X-ray diffraction (XRD) demonstrated that confinement also induced formation of thermodynamically less stable crystal phase [25]. For example, α-MoC$_{1-x}$ formed inside the SWNT channels while those species dispersed on the exterior walls of SWNTs were turned into β-Mo_2C, although exactly the same carburization conditions had been applied for both samples [26].

Fig. 2(a) displays the N_2 adsorption–desorption (Quantachrome NOVA 4200e) isotherms for these samples, which exhibit a hysteresis loop in the relative P/P_0 range from 0.85 to 1, indicating a meso-porous structure [27]. This is attributed to the secondary pores generated by the stacking of SWNTs. The specific surface area of blank SWNTs reaches as high as 1616 m^2 g^{-1}. Upon loading of Mo species, the surface area drops to 467 m^2 g^{-1} and 406 m^2 g^{-1}, for MoC$_x$@SWNT and MoC$_x$/SWNTs, respectively. This indicates that the carbon nanotube surface has been partially shielded by Mo species. Furthermore, some of the nanotube tips might be blocked or partially blocked by Mo species. The Raman spectra (LabRAM HR 800) in Fig. 2(b) show that all samples exhibit three characteristic

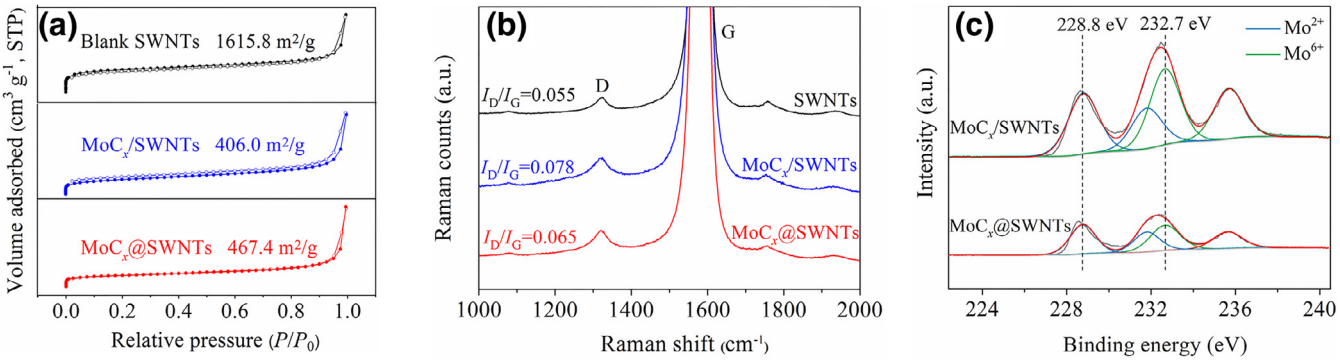

Fig. 2. Structural properties of MoC_x@SWNTs and MoC_x/SWNTs in comparison to the original SWNTs. (a) N_2 adsorption–desorption isotherms. (b) Raman spectra, which are normalized by the G band. (c) XPS Mo 3*d* spectra.

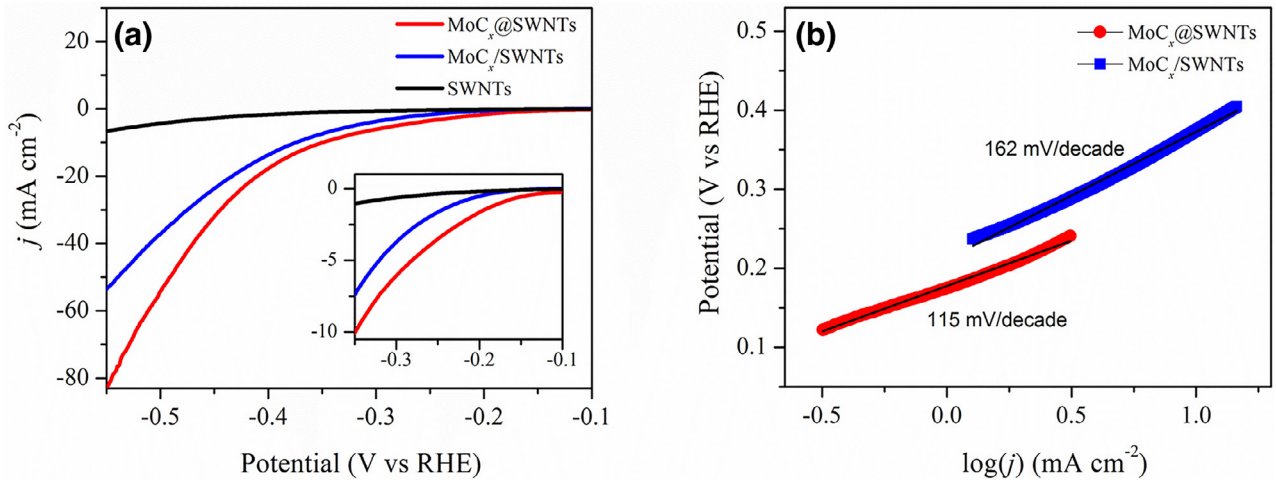

Fig. 3. (a) HER activities of MoC_x@SWNTs, MoC_x/SWNTs along with the blank SWNTs for comparison in 1 M $HClO_4$. The inset shows an enlarged section at low potentials. (b) Tafel plots of MoC_x@SWNTs and MoC_x/SWNTs.

peaks at 1325, 1585 and 1758 cm^{-1}. The former two correspond to the D and G bands of CNTs. The intensity ratio of the D to G band (I_D/I_G) is frequently used to evaluate the defect content of CNTs. It is seen that the blank SWNTs exhibit a very small I_D/I_G ratio (0.055), indicating the perfect structure of pristine nanotubes. For MoC_x@SWNT and MoC_x/SWNTs, the I_D/I_G ratio increases slightly to 0.065 and 0.078, respectively. This indicates that a small number of defects have been created on SWNTs upon loading of Mo species and the carburization process.

Our previous studies revealed that metal oxides tended to retain at a more reduced state than those dispersed on the outer surfaces, e.g. iron oxide [23], molybdenum oxide [25]. It is known that MoC_x is prone to oxidation upon exposure to air. Therefore, we examined the valence state distribution of MoC_x. X-ray photoelectron spectroscopy (XPS, Thermo Scientific ESCALAB 250Xi) analysis of the encapsulated MoC_x species (Fig. 2c) shows the presence of Mo^{2+} (corresponding to the signal of Mo $3d_{5/2}$ at 228.8 eV), in addition to Mo^{6+} (corresponding to the signal of Mo $3d_{5/2}$ at 232.7 eV) [28]. The high oxidation state of Mo^{6+} arises from oxidized Mo species, which is commonly observed as carbides are exposed to air, as reported previously [29]. Interestingly, the surface concentration of Mo^{2+} over MoC_x@SWNTs (51.1%) is higher than MoC_x/SWNTs (44.7%), suggesting that SWNT channels could hinder the surface oxidation of MoC_x NPs, which is consistent with our previous findings that the CNT-confined environment is beneficial to keep metal at a lower valence state [23,30].

The HER electrocatalytic activity of both MoC_x@SWNTs and MoC_x/SWNTs in acidic (pH = 0) aqueous solution is measured. For comparison, the blank SWNTs are also examined. The as-prepared catalysts were carefully dispersed on the glassy carbon electrodes with a mass loading of 0.32 mg cm^{-2}. The steady polarization curves in 1 M $HClO_4$ are presented in Fig. 3(a). It is seen that blank SWNTs sample exhibit a much poorer HER activity than both MoC_x@SWNTs and MoC_x/SWNTs. Furthermore, MoC_x@SWNTs is much more active than MoC_x/SWNTs. To achieve a current density of 10 mA cm^{-2}, MoC_x@SWNTs requires an over-potential (η) of 345 mV, which is 35 mV lower than MoC_x/SWNTs ($\eta = 380$ mV). The Tafel slopes, derived from fitting the Tafel plots to the Tafel equation ($\eta = b\log j + a$, where j is the current density and b is the Tafel slope), can provide additional information about activity and give insight into the reaction mechanism of HER [31]. As shown in Fig. 3(b), the Tafel slope of MoC_x@SWNTs is 115 mV dev^{-1}, which is much smaller than that of MoC_x/SWNTs (162 mV dev^{-1}), implying a superior performance of MoC_x@SWNTs. It is generally agreed that the HER process in acidic solution proceeds via two elementary steps [32]. The first one is the electrochemical reduction of hydrogen in aqueous (Volmer reaction, Eq. (1)), and the second one is the desorption of adsorbed hydrogen, which can proceed via either the ion and atom reaction (Heyrovsky reaction, Eq. (1)) or the atom combination reaction (Tafel reaction, Eq. (3)) [32]. According to previous reports, the Tafel slope values are 120, 40, and 30 mV dev^{-1} for Volmer, Heyrovsky, and Tafel steps being the rate de-

Table 1. Properties of different samples.

Sample	Mo loading[a] (wt%)	Average particle size[b] (nm)	Specific surface area[c] ($m^2\ g^{-1}$)
Blank SWNTs	–	–	1616
MoC_x@SWNTs	15.0	2.9	467
MoC_x/SWNTs	14.0	6.5	406

[a] Determined by inductively coupled plasma–optical emission spectrometry (ICP–OES, PerkinElmer ICP-OES 7300DV).
[b] Measured from TEM images.
[c] Determined by N_2 adsorption/desorption, using Brunner–Emmett–Teller (BET) method.

termining steps, respectively [33,34]. Therefore, the present result indicates that the HER process on MoC_x@SWNTs is controlled by the Volmer step, i.e. the electrochemical reduction of hydrogen.

$$H_3O^+ + e^- + {}^* \rightarrow H^* + H_2O \quad (1)$$

$$H_3O^+ + e^- + H^* \rightarrow H_2 + H_2O \quad (2)$$

$$H^* + H^* \rightarrow H_2 \quad (3)$$

It has been demonstrated that β-Mo_2C performed the highest activity in HER among all four phases of molybdenum carbide (α-MoC_{1-x}, η-MoC, γ-MoC, and β-Mo_2C) due to its more Pt-like Fermi level energy [35]. It is surprising that MoC_x@SWNTs is more active than MoC_x/SWNTs since MoC_x@SWNTs exhibits α-MoC_{1-x} phase and MoC_x/SWNTs exhibits β-Mo_2C phase. Therefore, there must be other factors which have contributed to the higher performance of MoC_x@SWNTs than MoC_x/SWNTs.

The HRTEM shows that the MoC_x@SWNTs exhibits much smaller MoC_x particles of 2.9 nm than that of MoC_x/SWNTs (6.5 nm, Fig. 1 and Table 1). It was reported previously that the particle size of MoC_x-based electrocatalysts could play a decisive role in their catalytic activity for HER [36–38]. For example, breaking down the micro-sized MoC_x to various nanostructures (e.g. nanooctahedrons, nanowires, nanoparticles) had been demonstrated to exhibit a significant effect on the HER activity [19,38–40]. Furthermore, the activity can be further enhanced by decreasing the size of MoC_x at the nanoscale. For example, Nakanishi and co-workers reduced the size of molybdenum carbonitride (MoCN) materials from hundreds of nanometers to 20–30 nm by utilizing a CO_2-emission assisted synthesis protocol, which consequently decreased the onset potential of HER from 90 to 50 mV [40]. Liu and coworkers reported that the MoC_x catalyst with particle sizes of 10–15 nm exhibited 3 times higher current density at an overpotential of 200 mV than that of 20–25 nm [38]. Zou and co-workers demonstrated that reducing the size of MoC_x particles from 7.3 to 3.6 nm could significantly enhance the HER activity [20]. A further reduction of MoC_x size from 1.5–4.5 nm to 1–3 nm by decreasing the annealing temperature could also improve HER activity, as demonstrated by Wang's group [41]. Therefore, the significantly smaller size of the encapsulated MoC_x NPs could be one of the reasons for the higher activity of MoC_x@SWNTs than MoC_x/SWNTs since smaller particles not only provide a larger amount of catalytic sites but also facilitate the access of electrolytes thereby enable rapid mass and charge transfer.

The BET specific surface area might be another factor influencing the HER catalysis, as reported widely in the literature [38,42]. The larger surface area of MoC_x@SWNTs would offer more reaction interfaces for the HER, thus resulting in the increased activity. In addition, XPS shows that MoC_x@SWNTs has a slightly higher Mo^{2+} concentration, which could also contribute to a higher HER activity, as the Mo^{2+} species have been reported to serve as the active site for HER [43–45]. On the other hand, the less Mo oxides (which are inactive for HER [18]) presence in MoC_x@SWNTs is beneficial to decrease the local resistance at the electrode–electrolyte interface, favoring a better activity.

Theoretically, the adsorption free energy of H ($\Delta G(H^*)$) can serve as a good measure for the catalytic activity of a catalyst for HER [20]. According to the volcano curve for the HER activity versus $\Delta G(H^*)$, the optimum value of $\Delta G(H^*)$ should be zero [46]. Previous density functional theory (DFT) calculation indicated that Mo metal itself possesses strong hydrogen binding energy due to the high position of its D-band electronic structure [39]. The adsorption can be weakened by carbonization Mo into MoC_x, but it is still too strong to achieve high activity [47]. Some approaches have been employed to optimize the electronic structure of MoC_x and thus the H adsorption on its surface, e.g. by introduction of doping elements [37] and construction of heteronanostructure [29]. In addition, it has been demonstrated that encapsulation of MoC_x within graphitic carbon layers could effectively tune the $\Delta G(H^*)$ to near zero [20,48,49]. The interaction between MoC_x and graphene shells can induce charge transfer from molybdenum to carbon, which further decreases the electron density on the carbide surface and downshifts the D-band center of Mo, and thereby decreases its hydrogen binding energy. Our previous study showed that the dissociative adsorption of gas molecules such as N_2 and O_2 on a series of metals can be weakened by encapsulation within SWNTs [50]. Therefore, the adsorption of hydrogen may be weakened too via encapsulation, consequently favors the electrochemical desorption of H^* and hence the HER kinetics.

However, the activity of MoC_x@SWNTs is lower than other reported MoC_x-based catalyst (Table 2) [18,20,39,51]. This is likely due to the low loading of Mo in MoC_x@SWNTs as well as the hydrophobic surface of SWNTs, which hampers its dispersion in aqueous solution and hence only limited contact surface. Nevertheless, the above results already demonstrate the advantage of encapsulation of MoC_x within SWNTs. Further improvement might be achieved by modification of the hydrophilic properties of the SWNT walls, which has been intensively investigated previously [52,53].

In summary, MoC_x NPs have been selectively dispersed either inside or outside SWNTs, and used as electro-catalysts for the HER in acid media. The electrochemical results indicate that MoC_x NPs encapsulated within SWNTs exhibit a higher HER activity compared with those dispersed on exterior walls. Characterization with

Table 2. Catalytic activity of various molybdenum carbide catalysts for HER.

Catalyst	Mo loading in catalysts (wt%)	Loading on the electrode (mg cm^{-2})	Electrolyte	η @ $j = 10$ mA cm^{-2} (mV)	References
MoC_x@SWNTs	15	0.32	1 M $HClO_4$	345	This work
Bulk Mo_2C	100	1.4	1 M H_2SO_4	210	[18]
Mo_2C NPs	100	0.102	0.5 M H_2SO_4	198	[51]
Mo_2C/CNT	30	2	0.1 M $HClO_4$	152	[39]
Mo_2C@NC	67	0.28	0.5 M H_2SO_4	124	[20]

BET, TEM, Raman spectroscopy and XPS reveals that SWNTs confined MoC_x catalysts possess a much smaller particle size, a larger specific surface area and a higher proportion of Mo^{2+} species. These factors are all beneficial for HER. In addition, the weakened adsorption of hydrogen on the encapsulated active sites may be another effect enhancing the HER activity.

Acknowledgments

We acknowledge the fruitful discussion with Prof. Guoxiong Wang from Dalian Institute of Chemical Physics. This work was financially supported by the National Natural Science Foundation of China (No. 21425312, 21688102, 21621063, and 21573224).

References

[1] J.A. Turner, Science 305 (2004) 972–974.
[2] M.S. Dresselhaus, I.L. Thomas, Nature 414 (2001) 332–337.
[3] X.X. Zou, Y. Zhang, Chem. Soc. Rev. 44 (2015) 5148–5180.
[4] C. Cheng, S.S.A. Shah, T. Najam, L. Zhang, X. Qi, Z. Wei, J. Energy. Chem. 26 (2017) 1245–1251.
[5] B. Luo, T. Huang, Y. Zhu, D. Wang, J. Energy Chem. 26 (2017) 1147–1152.
[6] X. Sun, J. Huo, Y. Yang, L. Xu, S. Wang, J. Energy Chem. 26 (2017) 1136–1139.
[7] Z. Zhou, N. Mahmood, Y. Zhang, L. Pan, L. Wang, X. Zhang, J.-J. Zou, J. Energy Chem. 26 (2017) 1223–1230.
[8] C. Tang, M.-M. Titirici, Q. Zhang, J. Energy Chem. 26 (2017) 1077–1093.
[9] J. Greeley, T.F. Jaramillo, J. Bonde, I.B. Chorkendorff, J.K. Norskov, Nat. Mater. 5 (2006) 909–913.
[10] H.B. Gray, Nat. Chem. 1 (2009) 7–7.
[11] H.H. Hwu, J.G.G. Chen, Chem. Rev. 105 (2005) 185–212.
[12] Y. Liu, T.G. Kelly, J.G.G. Chen, W.E. Mustain, ACS Catal. 3 (2013) 1184–1194.
[13] S. Li, C. Yang, Z. Yin, H. Yang, Y. Chen, L. Lin, M. Li, W. Li, G. Hu, D. Ma, Nano Res. 10 (2017) 1322–1328.
[14] M.A. Lukowski, A.S. Daniel, F. Meng, A. Forticaux, L.S. Li, S. Jin, J. Am. Chem. Soc. 135 (2013) 10274–10277.
[15] W.F. Chen, J.T. Muckerman, E. Fujita, Chem. Commun. 49 (2013) 8896–8909.
[16] Z.C. Xing, Q. Liu, A.M. Asiri, X.P. Sun, Adv. Mater. 26 (2014) 5702–5707.
[17] L. Lin, W. Zhou, R. Gao, S. Yao, X. Zhang, W. Xu, S. Zheng, Z. Jiang, Q. Yu, Y.-W. Li, C. Shi, X.-D. Wen, D. Ma, Nature 544 (2017) 80–83.
[18] H. Vrubel, X.L. Hu, Angew. Chem. Int. Ed. 51 (2012) 12703–12706.
[19] H.B. Wu, B.Y. Xia, L. Yu, X.Y. Yu, X.W. Lou, Nat. Commun. 6 (2015) 6512.
[20] Y.P. Liu, G.T. Yu, G.D. Li, Y.H. Sun, T. Asefa, W. Chen, X.X. Zou, Angew. Chem. Int. Ed. 54 (2015) 10752–10757.
[21] F.X. Ma, H.B. Wu, B.Y. Xia, C.Y. Xu, X.W. Lou, Angew. Chem. Int. Ed. 54 (2015) 15395–15399.
[22] H.L. Lin, Z.P. Shi, S.N. He, X. Yu, S.N. Wang, Q.S. Gao, Y. Tang, Chem. Sci. 7 (2016) 3399–3405.
[23] W. Chen, X. Pan, X. Bao, J. Am. Chem. Soc. 129 (2007) 7421–7426.
[24] F. Zhang, F. Jiao, X.L. Pan, K. Gao, J.P. Xiao, S. Zhang, X.H. Bao, ACS Catal. 5 (2015) 1381–1385.
[25] T. Cui, X. Pan, J. Dong, S. Miao, D. Miao, X. Bao, Nano Res. (2018). https://doi.org/10.1007/s12274-018-1975-2.
[26] J.S. Lee, L. Volpe, F.H. Ribeiro, M. Boudart, J. Catal. 112 (1988) 44–53.
[27] K.S.W. Sing, D.H. Everett, R.A.W. Haul, L. Moscou, R.A. Pierotti, J. Rouquerol, T. Siemieniewska, Pure Appl. Chem. 57 (1985) 603–619.
[28] X. Yang, X. Feng, H. Tan, H. Zang, X. Wang, Y. Wang, E. Wang, Y. Li, J. Mater. Chem. A 4 (2016) 3947–3954.
[29] H. Lin, Z. Shi, S. He, X. Yu, S. Wang, Q. Gao, Y. Tang, Chem. Sci. 7 (2016) 3399–3405.
[30] W. Chen, Z. Fan, B. Zhang, G. Ma, K. Takanabe, X. Zhang, Z. Lai, J. Am. Chem. Soc. 133 (2011) 14896–14899.
[31] F.-X. Ma, H.B. Wu, B.Y. Xia, C.-Y. Xu, X.W. Lou, Angew. Chem. Int. Ed. 54 (2015) 15395–15399.
[32] C.G. Morales-Guio, L.-A. Stern, X. Hu, Chem. Soc. Rev. 43 (2014) 6555–6569.
[33] B. Børresen, G. Hagen, R. Tunold, Electrochim. Acta 47 (2002) 1819–1827.
[34] B.E. Conway, B.V. Tilak, Electrochim. Acta 47 (2002) 3571–3594.
[35] C. Wan, Y.N. Regmi, B.M. Leonard, Angew. Chem. Int. Ed. 53 (2014) 6407–6410.
[36] B. Sljukic, M. Vujkovic, L. Amaral, D.M.F. Santos, R.P. Rocha, C.A.C. Sequeira, J.L. Figueiredo, J. Mater. Chem. A 3 (2015) 15505–15512.
[37] K. Xiong, L. Li, L. Zhang, W. Ding, L. Peng, Y. Wang, S. Chen, S. Tan, Z. Wei, J. Mater. Chem. A 3 (2015) 1863–1867.
[38] L. Liao, S. Wang, J. Xiao, X. Bian, Y. Zhang, M.D. Scanlon, X. Hu, Y. Tang, B. Liu, H.H. Girault, Energy Environ. Sci. 7 (2014) 387–392.
[39] W.F. Chen, C.H. Wang, K. Sasaki, N. Marinkovic, W. Xu, J.T. Muckerman, Y. Zhu, R.R. Adzic, Energy Environ. Sci. 6 (2013) 943–951.
[40] Y. Zhao, K. Kamiya, K. Hashimoto, S. Nakanishi, J. Am. Chem. Soc. 137 (2015) 110–113.
[41] R. Ma, Y. Zhou, Y. Chen, P. Li, Q. Liu, J. Wang, Angew. Chem. Int. Ed. 54 (2015) 14723–14727.
[42] J. Guo, J. Wang, Z. Wu, W. Lei, J. Zhu, K. Xia, D. Wang, J. Mater. Chem. A 5 (2017) 4879–4885.
[43] W.-F. Chen, J.T. Muckerman, E. Fujita, Chem. Commun. 49 (2013) 8896–8909.
[44] M.S. Faber, S. Jin, Energy Environ. Sci. 7 (2014) 3519–3542.
[45] D.H. Youn, S. Han, J.Y. Kim, J.Y. Kim, H. Park, S.H. Choi, J.S. Lee, ACS Nano 8 (2014) 5164–5173.
[46] J.K. Norskov, T. Bligaard, A. Logadottir, J.R. Kitchin, J.G. Chen, S. Pandelov, J.K. Norskov, J. Electrochem. Soc. 152 (2005) J23–J26.
[47] R. Michalsky, Y.J. Zhang, A.A. Peterson, ACS Catal. 4 (2014) 1274–1278.
[48] J. Deng, P. Ren, D. Deng, L. Yu, F. Yang, X. Bao, Energy Environ. Sci. 7 (2014) 1919–1923.
[49] H. Zhang, Z. Ma, G. Liu, L. Shi, J. Tang, H. Pang, K. Wu, T. Takei, J. Zhang, Y. Yamauchi, J. Ye, NPG Asia Mater 8 (2016) e293.
[50] J.P. Xiao, X.L. Pan, S.J. Guo, P.J. Ren, X.H. Bao, J. Am. Chem. Soc 137 (2015) 477–482.
[51] L. Ma, L.R.L. Ting, V. Molinari, C. Giordano, B.S. Yeo, J. Mater. Chem. A 3 (2015) 8361–8368.
[52] J. Chen, M.A. Hamon, H. Hu, Y.S. Chen, A.M. Rao, P.C. Eklund, R.C. Haddon, Science 282 (1998) 95–98.
[53] D. Tasis, N. Tagmatarchis, A. Bianco, M. Prato, Chem. Rev. 106 (2006) 1105–1136.